

Petrochemistry and Tectonic Evolutions of the Tertiary basalt along Red Sea Coast, Central Eastern Desert, Egypt

Yasmin M. Taher*, Asran M. Asran, A. El-Shater and Shaymaa Rizk

Geology Department, Faculty of Science, Sohag University, Sohag 82524, Egypt.

*Email: yasmin.mohammeed@gmail.com

Received: 17th January 2025, Revised: 2nd March 2025, Accepted: 5th March 2025

Published online: 24th April 2025

Abstract: To investigate the petrochemistry and genesis of Tertiary basalts in Egypt, which are among the most extensively distributed Tertiary basaltic flows in the region, nineteen basaltic samples were collected from basaltic rocks situated south of Qusier city, specifically in Wadi Sharm El Bahari, Wadi Sharm El Qiblli and Wadi Wizr along the Red Sea Coast. The samples were analyzed mineralogically and geochemically. The field investigation indicates that the basaltic rocks are oriented in a NW-SW direction, parallel to the Red Sea Rift. Petrographic analyses elucidate the existence of olivine basalts, porphyritic basalts, amygdaloidal olivine basalts and porphyritic olivine basalts. Some basalt flows exhibit slight alteration, showing the development of chlorite, serpentine, clay minerals and actinolite, along with the release of iron oxide. Geochemical data, encompassing major and trace elements, were evaluated. Variation diagrams validated that the basalts originated from partial melting and fractional crystallization. The significance of fractional crystallization processes, as opposed to crustal contamination processes, is accentuated by plotting Nb/Y versus Rb/Y. The Rb/Nb ratios (>2) signify the crustal compositions and melts, with the magma source originating from the OIB-source mantle. As indicated by discrimination diagrams, the basalts exhibit an alkaline to tholeiitic magma type and an orogenic, within-plate tectonic context. Their estimated crystallization temperatures range between 1180-1200°C. The oceanic characteristics of some basalt samples on the TiO₂-K₂O-P₂O₅ diagram indicate their association with the earliest rifting phase of the Red Sea.

Keywords: Geochemistry, Petrology, Tertiary Volcanism, Egypt.

1. Introduction

Tertiary sedimentation in Egyptian territory was interrupted by extensive volcanic activity and crustal movements, which were responsible for the formation of the Red Sea Graben. Magma penetrated the Oligocene and older rocks hundreds of kilometers apart in many localities. This resulted in the formation of isolated basaltic dykes, sheets and volcanic cones. A detailed presentation of these occurrences was studied [1,2]. It is almost certain that the active magma of all the Tertiary volcanoes of Lower Egypt was basaltic. Nevertheless, the types of eruptions varied from pure effusive and mixed to highly explosive and even cryptovolcanic [2]. Although these basalts may not be precisely contemporaneous, they constitute a mappable rock unit frequently taken as the upper limit of the Oligocene succession in Egypt.

Tertiary basalts occur in several locations in Egypt (Fig. 1), which shows the distribution of tertiary basaltic rocks [3], mainly in the eastern desert (Cairo-Suez District, Wadi Hodein, south Quseir, Abu Zaabal and East Samalut) and in the western desert (Gabal Qatrani, Baharyia Oasis, northeast of Gilf Kebir and North Gebel Uweinate). Intraplate basaltic volcanicity occurs in both continental and oceanic. Magma generated in the intraplate continent differs in composition from the oceanic crust, which is attributed to the variable composition of the continent [4]. There is no consensus among the researchers about the origin of the continental intraplate basalt concerning

the contribution of the mantle material, lithospheric mantle and asthenospheric mantle and their magma genesis as they are similar in composition to ocean island basalt. [5].

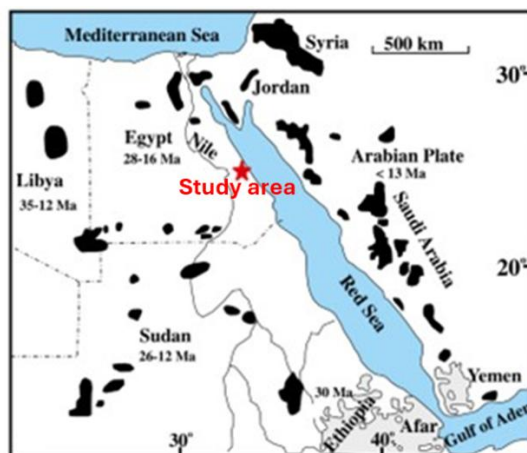


Figure 1: Distribution of tertiary basaltic rocks after [3].

Intraplate basaltic rocks are widely distributed in the Red Sea area due to the action of the lithospheric extensions and mantle plume activity [6]. The volcanic eruptions in Egypt during the Phanerozoic were associated with the Red Sea extension that started about 30 Ma ago during the Late Oligocene-Early Miocene and have been restricted to NNW to

SSW-trending rift valleys. These volcanic activities are formed as flow sheets, small hills and dikes.

Many authors have studied the presented area (e.g., [7-11]). Some researchers mentioned that the Precambrian rocks occupied the western part of the study area, claimed that there were no signs of contact thermal metamorphism in the overlying Miocene layers and characterized the volcanic events in Wadi Wizr as doleritic flows [8,11,12]. The exposures beneath, which are primarily composed of Cretaceous sandstones, show the heat impact of these lava flows.

The study region is the youngest unit of exposed basement rocks in Egypt's central-eastern desert. It is bounded by latitudes 25°43'~36.59''- 25°51'11.09''N and longitudes 34°24'05.31''- 34°19'32.23''E. It is situated south of the El Quseir Asphaltic Road (Fig. 2).

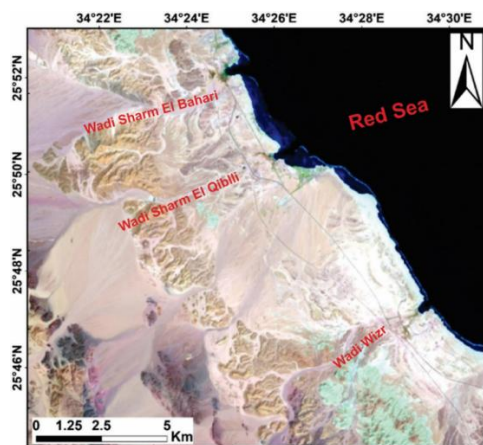


Figure 2: Location map of the study area.

To achieve our contribution to this study, integrated field petrographic and geochemistry data were presented on the occurrences along the Red Sea coast (Sharm El-Bahari, Sharm El-Qibli and Wadi Wizr). The main objectives are: 1) define and trace the geology and field characteristics of the basaltic rocks, 2) clarify the processes affecting the chemical composition of these rocks, 3) deduce the main character of the magma source, 4) assess the impact of crustal contamination on these magma samples and 5) outline the magmatic development of these basalts and the characteristics of their mantle source.

2. Geologic setting

The exposed rocks along the mainstream of Sharm El-Bahari, Sharm El-Qibli and Wadi Wizr are differentiated into a) Precambrian basement rocks and b) Phanerozoic rocks as shown in the geological map of the study area after [13] (Fig. 3). The Precambrian basement rocks are distinguished into ophiolitic rocks that occupy the upper streams of Wadi Wizr, which include serpentinite, meta-gabbro and meta-basalt [12].

These rocks and their pyroclastic equivalents are tectonically incorporated within the calc-alkaline metavolcanic rocks (Fig. 4a). These metavolcanic rocks are intruded by granitoid rocks, a meta-gabbro diorite complex and dyke swarms of intermediate to acidic composition (Fig. 4b). The calc-alkaline metavolcanic is differentiated into meta-

andesites, meta-basalts and their equivalent pyroclastics, with subordinate meta-dacites. It is highly sheared and transformed into tremolite schist and talc carbonates (Fig. 4c). Intrusive rocks are represented by the meta-gabbro diorite complex, granodiorite and granite (Fig. 4d). The intrusive rocks are commonly intruded into calc-alkaline metavolcanics. The meta gabbro diorite rocks display a greyish-green color and are intruded by granitoid rocks of light color. Phanerozoic rocks are represented by sedimentary rock succession and the basaltic lava flow. The sedimentary rocks include pre-rift sedimentary (Eocene-Cretaceous) Abu Ghusun Formation intercalated with Nakheil Formation (Oligocene), Ranga Formation (early Miocene), Um Mahara Formation (middle Miocene) and post-Middle Miocene sediments [3].



Figure 3: Geological map of the study area after [10].

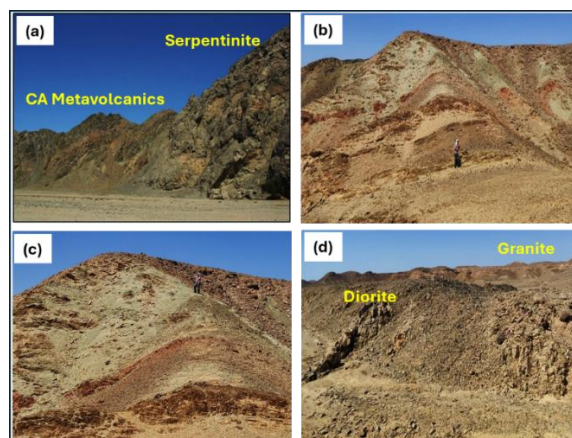


Figure 4: (a) Photograph showing calc-alkaline metavolcanic intruded by intermediate and acidic dyke swarms, (b) Photograph showing highly sheared metavolcanic, (c) Photograph showing serpentinite slices tectonically incorporated within the calc-alkaline metavolcanic and (d) Photograph showing granitoid rocks intruding into the meta-gabbro diorite complex.

Basaltic rocks are investigated at Wadi Sharm El-Bahari, Wadi Sharm El-Qiblli and Wadi Wizr, which are aligned in the NNW-SSE direction and conformable with the Red Sea trend. They overlain the Abu Ghusun Formation (Oligocene) siliciclastic sediments of variable color (reddish white to brick red) and underlain the Ranga Formation (Early Miocene). The visual estimation thickness of the Abu Ghusun Formation ranged from 3-5m and in some localities covered by rock screes and talus (Fig. 5a).

The lava flow caused induration and burning of the lower sedimentary succession (siliciclastic sedimentary composition). It is observed that talus and/or screes commonly conceal contact with the overlying rocks. However, well-exposed contact can be seen at Wadi Wizr, which dips 10–20 degrees toward the Red Sea coast. It is characterized by a reddish to whitish-grey layer about 70cm thick that overlies directly on the intensely weathered basalt flow.

Consequently, no contact metamorphism was observed on the overlying rocks; therefore, the observed caustic metamorphism produced compact, laminated, dark reddish-brown sandstone underlying rock, up to 15-20cm thick, close to the contact with the lava flow at Wadi Sharm El-Qiblli. (Fig. 5b).

The field investigations clarified the variable thickness of the basaltic rocks at the three localities. They suggested that the investigated basalts represent lava flow rather than sills and/or dykes due to: 1) The caustic (contact) metamorphism is on the underlying, not the overlying rocks. 2) The weathered contact zone of the upper lava flow surface (paleosol) at the base of early Miocene rocks is distinguished by its variable colors (reddish, grayish, whitish and brownish). 3) There are no penetrated apophyses into overlying rocks and/or sedimentary inclusion in the lava flow. 4) The presence of gas bubbles (vesicles) at the top of the lava flow, where the vesicles display different sizes and shapes (Fig. 5c). 5) It is observed that the lava flow is cut by irregular veins and/or veinlets that represent debris-washed carbonates into cracks in the lava flow (Fig. 5d).

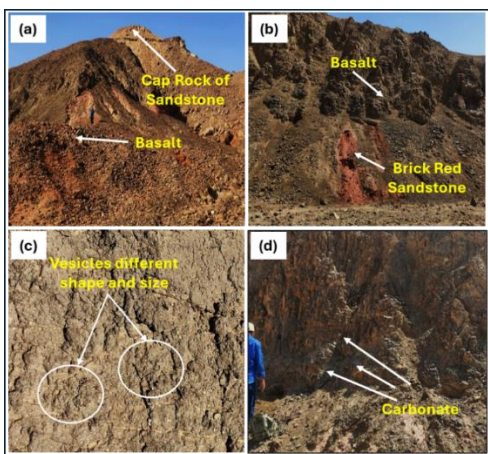


Figure 5: (a) Photograph showing the Abu Ghusun Formation (lower sedimentary succession) and the Ranga Formation (upper sedimentary succession), (b) Photograph showing compact, laminated, dark reddish-brown sandstone along the contact with the lava flow at Wadi Sharm El Qiblli, (c) Vesicles and amygdales exhibit irregular, elongated and rounded shapes and (d) Photograph showing lava flows that were cut by irregular veins and/or veinlets that represent debris-washed carbonates into cracks in the lava flow.

2. Materials and methods

Nineteen representative samples (three samples from Sharm El-Bahari, two from Sharm El Qiblli and fourteen from Wadi Wizr) were selected for a geochemical analysis. Major and trace element composition were determined using a Rigaku ZSX Primus IV, series IV Scanning X-Ray Fluorescence (XRF) analyzer at the Economic Geology Laboratory, Department of Earth Resources Engineering, Kyushu University (Japan). Samples were crushed and milled using a vibration mill, with loss of ignition (L.O.I) measured as the weight difference after ignition. The operating conditions of the XRF analysis were comprised of an accelerating voltage of 40 kV, a current of 40 mA, and gas stans is 35 ml/min. The JA-3 (Japan-igneous rocks standard) was used as the standard sample.

3. Petrography

3.1. Wadi Sharm El-Bahari:

Basaltic rocks at Wadi Sharm El-Bahari are differentiated petrographically into olivine basalt and porphyritic basalt.

A. Olivine basalt: In hand specimens, these rocks are dark grey to black, but the weathered samples display a brownish to greyish-brown color, fine-grained with plagioclase and/or olivine phenocrysts. Under the microscope, olivine basalt consists of plagioclase olivine and augite. Iron oxides are accessory minerals, whereas epidote and zoisite are common secondary minerals. These rocks display porphyritic, glomeroporphyritic, ophitic, diabasic and sub-ophitic textures (Fig. 6a-d).

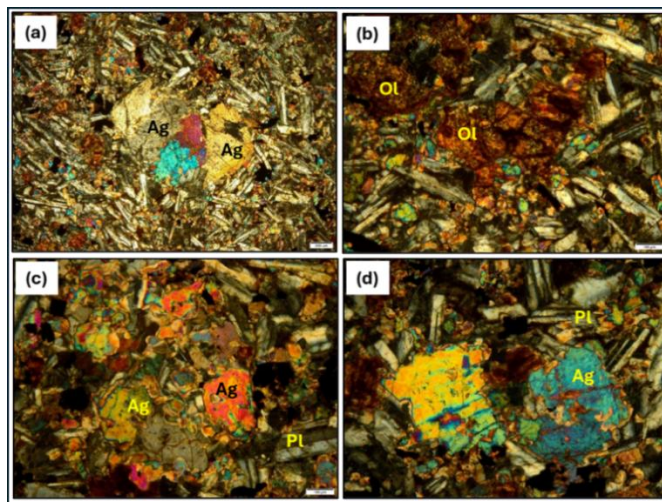


Figure 6: (a) Augite (Ag) phenocrysts clustered together and embedded in fine-grained groundmass display glomeroporphyritic texture (CN), (b) Olivine (Ol) phenocryst embedded in fine-grained groundmass displays porphyritic texture (CN) and (c&d) Augite phenocrysts are partially or completely enclosed plagioclase laths that conform to ophitic and subophitic textures (CN).

B. Porphyritic basalt: These rocks are dark grey to black in hand specimens, but the weathered samples are brownish to greyish-brown. They are fine-grained with plagioclase and/or olivine phenocrysts; some samples contain amygdales. Under the microscope, basalt consists essentially of plagioclase,

olivine and augite. Iron oxides are accessory minerals (Fig. 7a). These rocks display fluidal (flow) and interstitial textures (Fig. 7b), whereas epidote is a common secondary mineral (Fig. 7c).

3.2. Wadi Sharm EL-Qiblli:

Basaltic rocks at Wadi Sharm El-Qiblli are differentiated petrographically into Amygdaloidal or vesicular Olivine basalt, Olivine basalt and porphyritic basalt.

A. Amygdaloidal Olivine basalt: In hand specimens, these rocks are dark grey to black, but the weathered samples are brownish to greyish brown. They are fine-grained with plagioclase and/or olivine phenocrysts and some samples contain vesicular and/or amygdaloids. Under the microscope, amygdaloidal olivine basalt consists essentially of plagioclase, olivine and augite. Iron oxides are accessory minerals, whereas epidote, chlorite and zoisite are common secondary minerals filled with amygdalus. These rocks display amygdaloidal textures (Fig. 7d).

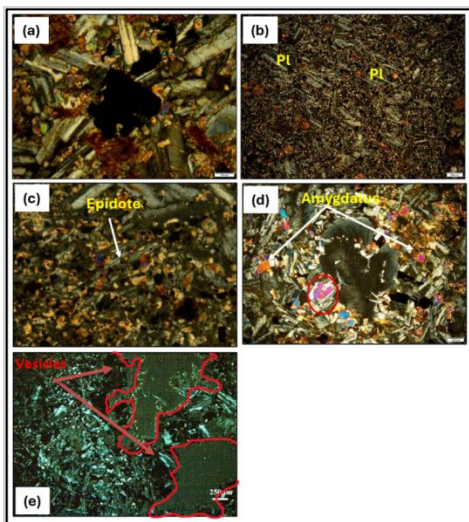


Figure 7: (a) Iron oxides are frequently disseminated throughout these rocks (CN), (b) Plagioclase (pl) crystals display flow and interstitial textures, (c) Picture showing numerous epidote aggregates (CN), (d) Amygdaloidal texture, which vesicles filled with secondary minerals and (e) Vesicular Texture in vesicular basalt (CN).

B. Olivine basalt: In hand specimens, these rocks are dark grey to black, but the weathered samples display a brownish to greyish-brown color, fine-grained with plagioclase and/or olivine phenocrysts. Under the microscope, olivine basalt consists essentially of plagioclase, olivine and augite. Iron oxides are accessory minerals, whereas epidote and zoisite are common secondary minerals.

C. porphyritic olivine basalt: In hand specimens, these rocks are dark grey to black, but the weathered samples display a brownish to greyish-brown color, fine-grained with plagioclase and/or olivine phenocrysts. Under the microscope, olivine basalt consists of plagioclase, olivine and augite. Iron oxides are accessory minerals, whereas epidote and zoisite are common secondary minerals.

3.3. Wdi Wizr:

Basaltic rocks at Wadi Wizr are differentiated

petrographically into four rock types: olivine basalt, basalt, vesicular basalt and amygdaloidal olivine basalt.

A. Olivine basalt: In hand specimens, these rocks are dark grey to black, but the weathered samples are brownish to greyish-brown. They are fine-grained, with plagioclase and/or olivine phenocrysts embedded in a fine-grained groundmass. In the thin section, olivine basalt consists essentially of plagioclase, olivine, and augite as phenocrysts embedded in fine-grained groundmass composed of plagioclase. Iron oxides are accessory minerals, whereas epidote, chlorite, and zoisite are common secondary minerals.

B. basalt: In hand specimens, these rocks are dark grey to black, but the weathered samples are brownish to greyish brown, fine-grained with plagioclase phenocryst. Under the microscope, basalt consists essentially of plagioclase, actinolite and chlorite. Iron oxides are accessory minerals, whereas epidote is a common secondary mineral.

C. Vesicular basalt: In hand specimens, these rocks are dark grey to black, but the weathered samples are brownish to greyish-brown. They are fine-grained with plagioclase phenocryst and contain vesicular. Under the microscope, vesicular basalt consists essentially of plagioclase and iron oxides are accessory minerals. These rocks display vesicular textures. (Fig. 7e)

D. Amygdaloidal Olivine basalt: In hand specimens, these rocks are dark grey to black, but the weathered samples are brownish to greyish brown. They are fine-grained with plagioclase and/or olivine phenocrysts; some samples contain amygdaloids. Microscopically, amygdaloidal olivine basalt consists essentially of plagioclase, olivine and augite phenocrysts. Iron oxides are accessory minerals, whereas epidote and zoisite are common secondary minerals. The description of the minerals that constitute the basaltic rocks is discussed in the following sections:

- 1- Plagioclase (Pl):** Plagioclase crystals (An42-50, An50-54, and An65-69) are distinguished into two generations; the early plagioclase generation forms subhedral to euhedral prismatic phenocrysts that range in size from crystals of 0.081x0.27 mm to 2.43x3.13 mm and are characterized by the twinning of lamellar, albite, Carlsbad and pericline types, besides zoning (Fig. 8a). Some plagioclase crystals are partial to completely altered to epidote, zoisite and clay minerals (smectite) (Figs. 8b). The second generation is represented by subhedral, fine-grained laths frequently concentrated in the groundmass. The microscopically identified plagioclase phenocrysts ranged in composition from andesine to labradorite and flowerer and the identification of plagioclase clarifies the presence of anorthite, labradorite, bytownite and albite. The latter may represent the attribution product of the calcic plagioclase and/or plagioclase of some groundmass.
- 2- Olivine (Ol):** It occurs as equant, fractured, rhombohedral, anhedral to subhedral crystals with the characteristic Y cracks, and the altered varieties display mesh texture (Fig. 8c). Olivine crystals are commonly altered to Iddingsite (reddish brown), limonite (lemon or honey yellow) and serpentine

minerals along the boundaries and Y cracks, where iron oxides are frequently concentrated.

- 3- **Augite (Ag):** Occurs as anhedral to subhedral phenocrysts ranging from 0.27x0.32 mm to 0.59x0.86 mm, enclosing completely or partially small laths of plagioclase feldspar, which give rise to the ophitic and sub-ophitic texture (Fig. 6a). Augite crystals are clustered together, conforming to the well-known glamero-porphyritic texture.
- 4- **Hypersthene (Hy):** It occurs as anhedral to subhedral prismatic phenocrysts 1.35x2.16 mm, yellow interference color, with first-order parallel extinction (Fig. 8d).
- 5- **Actinolite (Act):** It occurs as anhedral to subhedral tabular prismatic crystals that commonly enclose plagioclase laths in ophitic and sub-ophitic fashion (Fig. 8e).
- 6- **Chlorite (Chl):** Frequently dispersed throughout these rocks, they form anhedral crystals with a pale green color and faint pleochroism (Fig. 8f). It is commonly grown at the expense of pyroxene and/or olivine.
- 7- **Iron Oxides:** They occur as irregular, small granules or, skeletal crystals that disseminate throughout these rocks and concentrate along the y cracks of olivine and and cleavage planes of pyroxene.

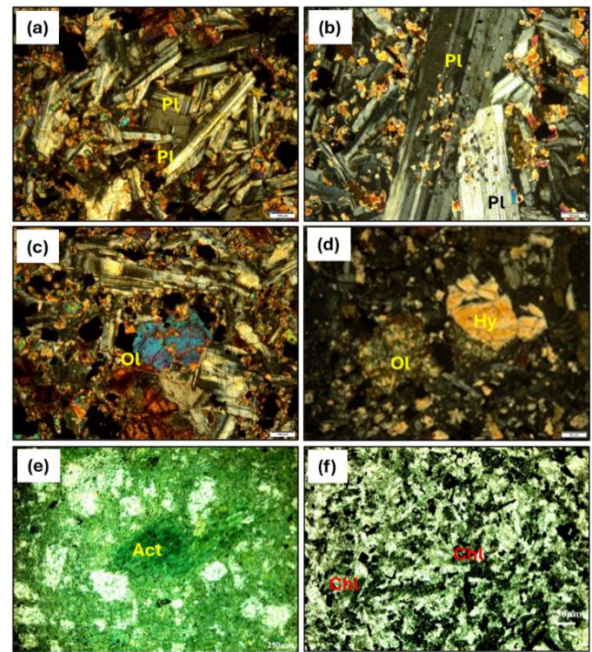


Figure 8: (a) Plagioclase (Pl) phenocrysts showing three types of twinning, such as lamellar, albite-Carlsbad, and pericline twinning, in addition to zoning (CN), (b) Plagioclase phenocrysts display altered cores and fresh rims where the alteration products are epidote, zoisite, and clay minerals, (c) plagioclase and olivine phenocrysts that are partially or completely altered, where the former is altered to epidote, zoisite, and clay minerals, but olivine is altered to Iddingsite (CN), (d) Hypersthene (Hy) phenocryst, (e) Display actinolite phenocryst, (f) Chlorite (Chl) phenocryst filled the overview.

Table 1: Major oxides in (Wt%)

S. N.	SiO ₂	TiO ₂	Al ₂ O ₃	Fe ₂ O ₃	MnO	MgO	CaO	Na ₂ O	K ₂ O	P ₂ O ₅	L.O.I.
1	44.12	2.815	13.910	17.686	0.211	6.359	6.951	3.040	0.859	1.143	2.26
2	49.88	2.145	14.603	13.092	0.192	6.793	4.922	4.228	0.209	0.618	2.6
3	48.99	2.415	14.992	14.905	0.106	4.822	7.658	2.591	1.500	0.278	1.17
4	50.15	2.47	14.477	14.644	0.097	5.273	5.905	3.018	1.705	0.278	2.07
5	48.66	2.964	12.983	13.762	0.163	7.202	9.365	1.834	1.357	0.307	1.26
6	46.01	2.503	13.746	12.818	0.186	7.991	12.043	1.736	1.223	0.368	1.37
7	47.92	1.998	14.954	13.478	0.146	6.839	8.454	2.927	0.923	0.376	1.47
8	48.49	2.296	13.929	14.792	0.168	5.909	8.973	1.943	1.289	0.34	1.46
9	49.06	2.318	12.717	11.819	0.12	9.945	7.875	2.573	0.953	0.315	1.86
10	48.08	1.382	14.426	13.229	0.165	8.352	8.102	2.163	1.031	0.356	2.25
11	47.59	2.469	13.233	12.877	0.282	9.331	7.512	2.447	0.93	0.378	2.71
12	44.97	1.995	11.902	14.375	0.221	8.811	10.792	1.837	0.877	0.359	1.75
13	53.58	0.499	14.728	10.729	0.181	5.949	9.735	1.817	0.214	0.152	1.79
14	49.53	2.374	13.664	11.789	0.221	6.219	8.803	3.238	0.802	0.459	2.18
15	50.43	2.526	14.356	9.979	0.113	7.823	6.427	3.506	1.373	0.381	1.91
16	49.22	2.746	15.124	11.393	0.18	6.277	8.638	3.439	0.94	0.45	1.24
17	49.07	2.727	14.704	11.885	0.144	5.892	8.891	3.268	1.036	0.345	1.55
18	49.59	2.159	15.505	11.247	0.155	5.064	9.162	3.497	0.883	0.409	1.45
19	48.63	1.891	13.966	10.729	0.123	8.536	9.792	2.905	1.072	0.451	1.26

Table 2: Trace elements concentration in (ppm)

S. N.	V	Cr	Co	Ni	Cu	Zn	Pb	Rb	Y	Sr	Ba	Zr	Nb	W	Th	Hf
1	354	33	32	44	20	324	10	13	44	397	359	264	30	5	0	7
2	289	15	26	26	27	249	18	3	50	537	138	364	15	3	0	11
3	343	128	24	46	28	262	12	27	36	1110	308	278	28	2	3	8
4	330	133	22	42	49	253	11	31	37	651	321	288	29	2	2	8
5	283	98	28	47	32	246	13	32	39	461	313	383	25	2	2	11
6	297	78	28	49	34	252	13	27	39	535	326	279	23	2	5	8
7	275	58	27	51	23	238	10	31	33	515	259	218	19	3	2	6
8	309	90	23	46	29	252	14	27	40	442	332	351	28	3	5	10
9	304	90	40	54	104	233	9	28	33	509	266	242	23	0	3	6
10	258	65	35	50	66	216	8	27	37	623	284	250	22	0	4	7
11	242	41	33	54	71	235	8	24	35	597	351	216	19	2	4	5
12	233	51	37	49	57	225	7	24	34	829	260	214	18	5	4	5
13	249	43	25	27	13	227	8	2	13	455	115	52	1	2	1	1
14	338	51	27	37	80	383	7	19	44	860	390	304	30	1	6	8
15	374	87	33	59	14	212	9	33	28	439	319	284	27	1	4	8
16	283	48	30	50	31	243	8	21	32	435	276	205	18	1	3	5
17	327	61	32	48	26	236	5	25	36	389	285	244	24	2	3	7
18	357	72	31	45	6	247	11	21	33	396	283	208	20	5	5	6
19	252	65	32	48	7	222	8	26	33	np	np	238	21	1	4	7

Table 3: The calculated CIPW norm for the analyzed Sharm Qiblli and Sharm Bahari sites.

Norm	Sharm Qiblli		Sharm Bahari		
	15	16	17	18	19
Q	0.53	0.2	0.77	1.03	0
or	7.67	5.12	5.64	4.85	5.88
ab	27.98	26.75	25.42	27.42	22.79
an	18.27	21.19	20.58	22.23	20.3
Di wo	4.07	6.61	7.59	7.4	9.33
Di en	3.01	4.56	5.08	4.69	6.64
Di fs	0.66	1.51	1.92	2.23	1.85
Hy en	15.46	9.89	8.47	7.05	6.78
Hy fs	3.38	3.28	3.21	3.34	1.89
Ol fo	0	0	0	0	4.47
Ol fa	0	0	0	0	1.38
Mt	13.66	15.2	15.86	15.13	14.44
He	0	0	0	0	0
Il	4.53	4.8	4.77	3.81	3.33
Ap	0.79	0.9	0.69	0.83	0.91
total	100	100	100	100	100

Table 4: The calculated CIPW norm for the analyzed Wadi Wizr site.

	Wadi Wizr													
	1	2	3	4	5	6	7	8	9	10	11	12	13	14
Norm	15	16	17	18	19	15	16	17	18	19	18	19	18	19
Q	0	1.86	3.49	3.59	3.87	0	0	4.28	0.31	0.93	0.2	0	11.63	2.1
or	4.5	1.14	7.94	9.07	7.23	6.57	4.96	6.84	5.2	5.59	5.06	4.76	1.18	4.4
ab	22.73	32.95	19.61	22.94	13.97	13.32	22.46	14.74	20.07	16.74	19.04	14.23	14.32	25.41
an	19.24	18.65	22.21	18.78	20.86	23.66	22.61	22.83	18.74	24.33	20.57	19.81	29.24	18.89
Di wo	2.24	0.22	4.33	2.55	8.1	11.95	5.63	6.41	6.52	4.42	4.89	11.42	6.25	8
Di en	1.29	0.14	2.43	1.5	5.43	8.19	3.57	3.81	4.74	2.88	3.43	7.52	3.78	5.29
Di fs	0.84	0.06	1.72	0.93	2.04	2.79	1.69	2.25	1.17	1.23	1.04	3.07	2.13	2.12
Hy en	9.33	15.51	8.37	10.36	10.79	5.4	10.83	9.44	18.21	16.25	18.05	7.71	10.09	9.14
Hy fs	6.06	6.96	5.91	6.43	4.05	1.84	5.13	5.58	4.5	6.96	5.47	3.14	5.67	3.66
Ol fo	2.41	0	0	0	0	3.18	0.79	0	0	0	0	3.47	0	0
Ol fa	1.73	0	0	0	0	1.19	0.41	0	0	0	0	1.56	0	0
Mt	22.69	17.5	19.35	19.1	17.98	16.87	17.74	19.25	15.82	17.57	17.19	19.11	14.51	15.87
He	0	0	0	0	0	0	0	0	0	0	0	0	0	0
Il	4.73	3.76	4.11	4.22	5.07	4.32	3.45	3.91	4.07	2.4	4.32	3.48	0.88	4.19
Ap	2.21	1.24	0.54	0.55	0.6	0.73	0.75	0.67	0.63	0.71	0.76	0.72	0.31	0.93
Total	100	100	100	100	100	100	100	100	100	100	100	100	100	100

4. Geochemistry

Tables (1,2) list the bulk rock geochemistry major and trace element and the representative nineteen basaltic samples from the Red Sea Coast basalt that were investigated at Wadi Sharm el Bahari, Wadi Sharm el Qiblli and Wadi Wizr Central Eastern Desert. In addition, the calculated CIPW norm (Tables 3,4) and various geochemical ratios and parameters are also presented. The chemically analyzed basaltic rocks reveal that SiO₂ content ranges from 44.124% to 53.577%, with an average of 48.36%, from 49.222% to 50.434%, with an average of 49.828% and from 48.626% to 49.589%, with an average of 49.095%, for Wadi Wizr, Wadi Sharm El-Qiblli and Wadi Sharm El-Bahari, respectively.

CaO content ranges from 4.922% to 12.043%, with an average of 8.364%, from 6.427% to 8.638%, with an average of 7.533% and from 8.891% to 9.792%, with an average of 9.282% for Wadi Wizr, Wadi Sharm El-Qiblli and Wadi Sharm El-Bahari, respectively.

Al₂O₃ content ranges from 11.902% to 14.992%, with an average 13.876%, from 14.356% to 15.124%, with an average of 14.74% and from 13.966% to 15.505%, with an average of 14.725% for Wadi Wizr, Wadi Sharm El-Qiblli and Wadi Sharm El-Bahari, respectively.

TiO₂ content ranges from 2.964% to 0.499%, with an average of 2.189%; from 2.526% to 2.746%, with an average of 2.636% and from 1.891% to 2.727%, with an average of 2.259% for Wadi Wizr, Wadi Sharm El-Qiblli and Wadi Sharm El-Bahari, respectively.

Fe₂O₃ content ranges from 10.729% to 17.686%, with an average of 12.515%, from 9.979% to 11.393%, with an average of 10.686% and from 10.729% to 11.885%, with an average of 11.287% for Wadi Wizr, Wadi Sharm El-Qiblli and Wadi Sharm El-Bahari, respectively.

MnO content ranges from 0.097% to 0.282% with an average of 0.176%, from 0.113% to 2.042% with an average of 0.778% and from 0.123% to 0.55%, with an average of 0.141% for Wadi Wizr, Wadi Sharm El-Qiblli and Wadi Sharm El-Bahari, respectively.

MgO content ranges from 9.945% to 4.822% with an average of 7.117%, from 6.277% to 7.283% with an average of 7.05% and from 5.064% to 8.536% with an average of 6.497% for Wadi Wizr, Wadi Sharm El-Qiblli and Wadi Sharm El-Bahari, respectively.

Na₂O content ranges from 1.736% to 4.228% with an average of 2.528%, from 3.439% to 3.506% with an average of 3.473% and from 2.905% to 3.497%, with an average of 3.223% for Wadi Wizr, Wadi Sharm El-Qiblli and Wadi Sharm El-Bahari, respectively.

K₂O content ranges from 0.209% to 1.705% with an average of 0.991%, from 0.94% to 1.373% with an average of 1.157% and from 0.883% to 1.036% with an average of 0.997% for Wadi Wizr, Wadi Sharm El-Qiblli and Wadi Sharm El-Bahari, respectively.

P₂O₅ content ranges from 0.152% to 1.143% with an average of 0.419%, from 0.45% to 0.381% with an average of 0.416% and from 0.345% to 0.451% with an average of 0.402% for Wadi Wizr, Wadi Sharm El-Qiblli and Wadi Sharm El-Bahari, respectively.

The field observation of the basalt flows shows that their susceptibility to the weathering process is variable. The absence of the unconformity contact between these flows indicates a short hiatus between them. This is attributed to the weathering process's effect on some major oxides, while MgO and FeO are more or less immobile (stable). In the crystallization of basaltic magma, MgO plays a significant role in their evolution since MgO enters the early-formed minerals such as olivines and pyroxenes and consequently, MgO is continuously depleted. Therefore, MgO content is considered directly or indirectly as MgO/FeO, which refers to the degree of differentiation [14]. The authors applied the MgO versus the major oxides and trace elements in the Harker diagram (Figs. 9,10). Adopting MgO content as a differentiation index (DI), major oxides display scattered trends. Increasing TiO₂, CaO, and P₂O₅ and decreasing Fe₂O₃, Al₂O₃ and SiO₂ with increasing degree of differentiation. Ni and Cr show a regression trend, indicating olivine and clinopyroxene fractionation and V displays a marked trend that decreases with increasing MgO, reflecting Fe-rich pyroxene fractionations. Sr shows the variable distribution.

The analyzed samples were plotted on the standard diagram, such as TAS (Fig. 11a) [15]. Plotted samples showed that Wadi Wizr and Sharm El-Qiblli data fall mostly along the dividing line between the basalt-picrite field, except sample (No. 13) from the Wadi Wizr area falls within the basaltic-andesite field and sample (No. 1) from Wizr basalt falls mainly within the picrite field. In addition, the alkali-lime index proposed by [16] was used, indicating that all samples fall mainly within the alkali field, except sample (No. 13) from the Wadi Wizr area, which falls within the alkali-calcic field (Fig. 11b) [16]. This is due to the enrichment of the carbonate material that fills the cavities and forms the amygdaloidal texture, as described in the thin section.

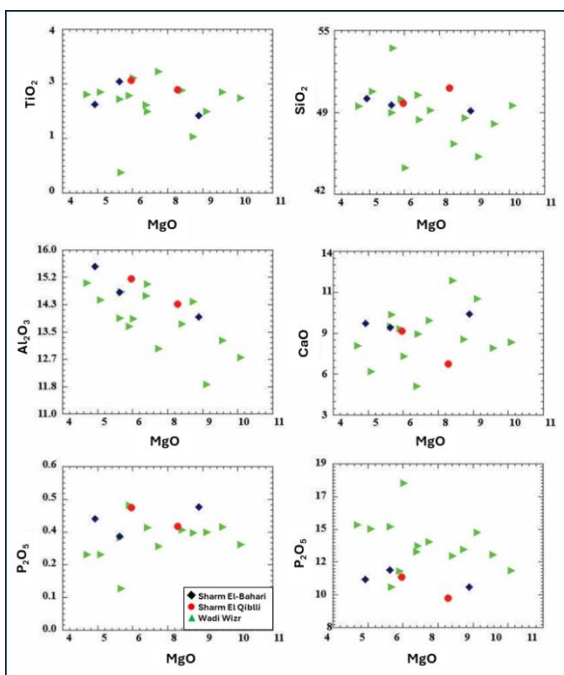


Figure 9: Harker variation diagrams for major oxides in (wt%) plotted against MgO (in wt%).

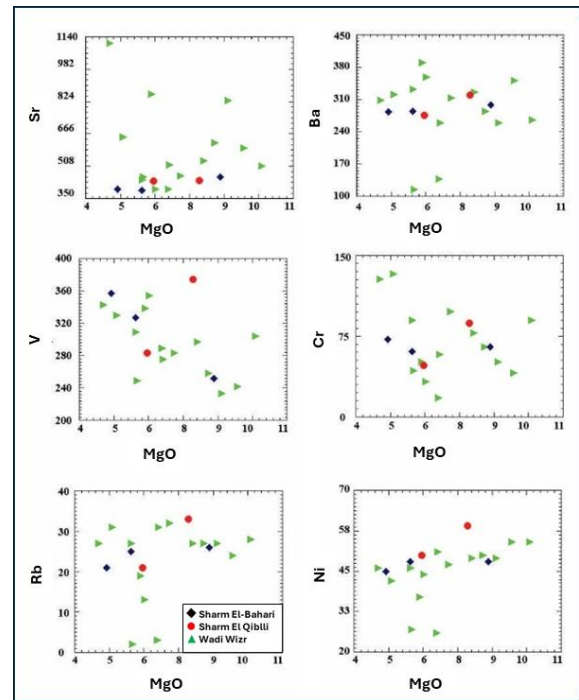


Figure 10: Harker variation diagrams for trace elements in (ppm) plotted against MgO (in wt%).

5. Magma Type

On the TAS diagram (Fig. 11c) [17], the analyzed samples fall on the dividing line between alkaline and sub-alkaline, except some samples are shifted from the dividing line. Furthermore, the analyzed samples are plotted on the alkalis against alumina (Fig. 11d) [18], where the Wadi Wizr basalt falls in the tholeiitic and alkali basalt fields. In contrast, Sharm El-Qiblli and Sharm El-Bahari basalts fall mainly within the alkali basalt field. On the alkalis against silica diagrams (Fig. 12a) [19], the plotted samples fall mainly within the high-aluminum basalt field. On the P₂O₅-Zr diagram (Fig. 12b) [20], the analyzed basaltic rocks fall within the alkali and tholeiitic basalt field. In addition, on the AFM diagram (Fig. 13a) [21], it is clear that the plotted samples of Wadi Wizr have an iron enrichment trend and fall mainly within the tholeiitic (TH) field. In contrast, Wadi Sharm El-Qiblli and Wadi Sharm El-Bahari samples are plotted within calc-alkaline and along the boundary between the tholeiitic and calc-alkaline fields. According to Powers [22], MgO content reflects the crystallization temperature of basaltic magma, assuming that all other parameters are constant. The temperature of the basaltic magma reveals that the Sharm El-Bahari, Sharm El-Qiblli and Wadi Wizr fall within the low-temperature fractionation stage LS (1190°C-1180°C), except some samples of Wadi Wizr fall within the field of the temperature between 1200-1190°C. From ordinary basic magma in which olivine, plagioclase and pyroxene separate, two other petrochemical parameters, viz., the iron ratio (normative Ab)/(normative Ab+An), are recognized as indicators of the extent of fractionation. Plotting the analyzed samples on the albite ratio against the iron ratio diagram (Fig. 13b) [23].

6. Tectonic setting:

The distribution of major and trace elements is used to detect the tectonic setting under which magmatic rocks erupted. Plotting the analyzed basalt samples on the Zr/Y versus Zr diagram (Fig. 14a) [24], the (2*Nb, Zr/4, and Y) diagram (Fig. 14b) [25] and the Zr/Y–Ti/Y discrimination diagram (Fig. 15a) for basalts [26] reveals that the analyzed samples fall mainly within the plate field. K₂O, TiO₂ and P₂O₅ distribution may be used to distinguish oceanic from non-oceanic basalts [27]. Plotting the analyzed basalt samples on the K₂O–TiO₂–P₂O₅ ternary diagram (Fig. 15b) [27] reveals that the analyzed basalt from the studied three localities falls close to the boundary line separating oceanic from non-oceanic basalts (continental basalt). These features established the activity accompanying the Red Sea's rifting and forming a new oceanic crust.

7. Discussion

7.1. Fractional crystallization:

The petrography description suggests that fractional crystallization processes controlled the evolution of the studied basalts due to: 1) The basalt rocks are generally porphyritic and the phenocrysts gradually change from olivine through olivine-clinopyroxene to olivine-clinopyroxene plagioclase. 2) The geochemical characteristics on the variation diagram (Fig. 10) display that the compatible Cr and Ni increased and Ba, Sr and Rb decreased with increasing MgO, suggestion olivine, clinopyroxene and plagioclase fractionation. 3) The well-defined Fe₂O₃, TiO₂ and P₂O₅ trend is attributed to Fe-Ti oxides and apatite crystallization.

7.2. Crustal contamination:

It is essential to infer the crust's contribution to the chemical composition of the studied basalt before discussing its source magma from the chemical analyses. The studied basalts have porphyritic and glomeroporphyritic textures, suggesting that the magma paused in crustal magma chambers before the eruption and thus had enough time to interact with the continental crust. However, the predominance of unaltered olivine within the basaltic rocks argues against the opportunity of the interaction with the crustal rocks. The significant ion lithophile elements (LILE) (such as Rb, Ba, K) and the high-field strength elements (HFSE) (such as Zr, Nb, Y) are incompatible with the phenocrysts mineral phase (such as olivine, clinopyroxene and plagioclase) in the examined basaltic rocks [28,29] mentioned that ratios, such as Rb/Zr, K/Rb and Ba/Nb don't display any variation by simple fractional crystallization where variations in these ratios are attributed to crustal contamination by the assimilation-fractional crystallization (AFC) process. In the investigated basaltic rocks, the ratio Rb/Zr and Ba/Nb show no apparent variations with decreasing MgO along the line labeled (crustal contamination), indicating that fractional crystallization processes play a significant role during the evolution of the studied rocks (Fig. 16a) [30] the absence of such a trend infer that crustal contamination did not play a significant role in the evolution of investigated basalts.

The role of the fractional crystallization processes rather than crustal contamination processes is enhanced by plotting Nb/Y versus Rb/Y diagram (Fig. 16b) [30,31], where Rb/Nb ratios indicate the crustal compositions and crustal melts (>2). In (Fig. 16b) [30,31], all of the plotted samples fall away from the upper and the lower crustal values and have very low Rb/Nb ratios [31]. Consequently, it is unreasonable to imagine that crustal contamination was superimposed on crystal fractionation in the evolution of the studied basalt.

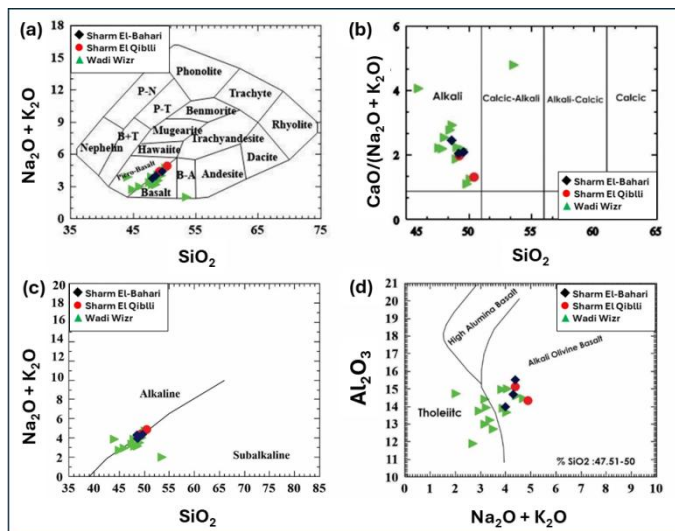


Figure 11: (a) Plots of analyzed samples on the total alkalis (Na₂O+K₂O) versus (TAS) diagram of (after [15]), (b) Plotted of analyzed samples on the standard diagram, such as the alkali-lime index proposed by [16], c) Plotted of analyzed samples on the standard diagram (TAS) diagram proposed by [17] and (d) Plotted of analyzed samples on the alkalis against alumina diagram proposed by [18].

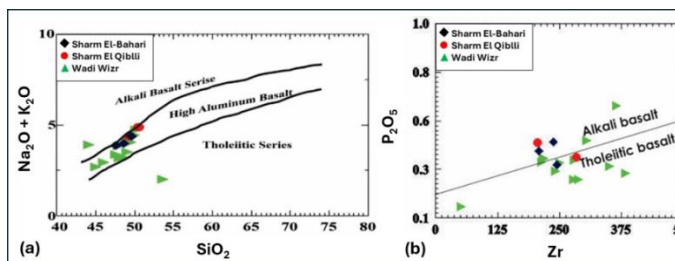


Figure 12: (a) Plotted of analyzed samples on the standard diagram Alkali vs SiO₂ proposed by [19] and (b) Plotted the analyzed samples using the P₂O₅ – Zr discrimination diagram for basalts (after [20]).

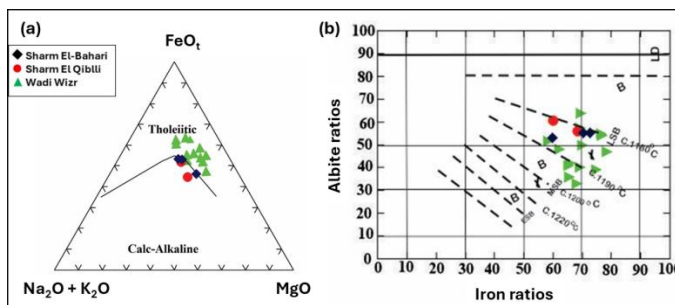


Figure 13: (a) Plotting of the samples analyzed on the AFM diagram (after [21]), (b) Plot the analyzed samples using the albite ratio against the iron ratio diagram. (after [23]).

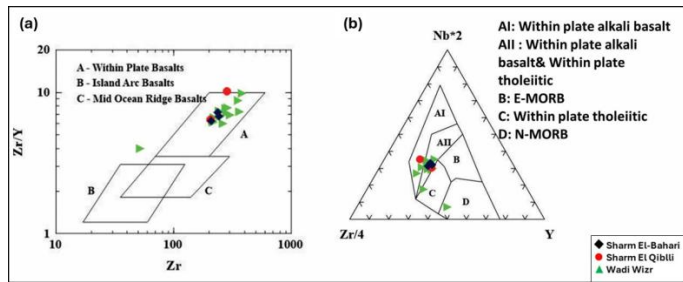


Figure 14: (a): Plotting of the analyzed samples on the Zr/Y versus Zr diagram (after [24]) and (b) Plotting of the analyzed samples on the (2*Nb, Zr/4 and Y) ternary diagram (after [25]).

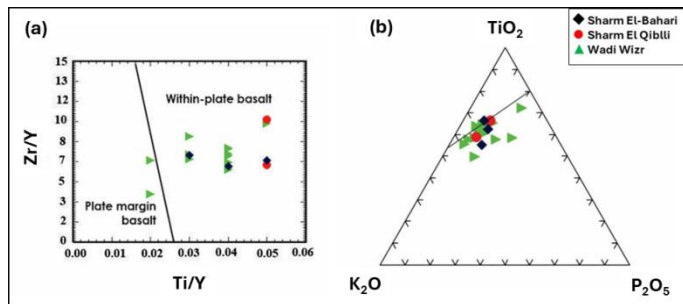


Figure 15: (a) Plotting of the analyzed samples on The Zr/Y – Ti/Y discrimination diagram for basalts [26] and (b) Plotting of the analyzed samples on the K₂O -TiO₂-P₂O₅ ternary diagram [27].

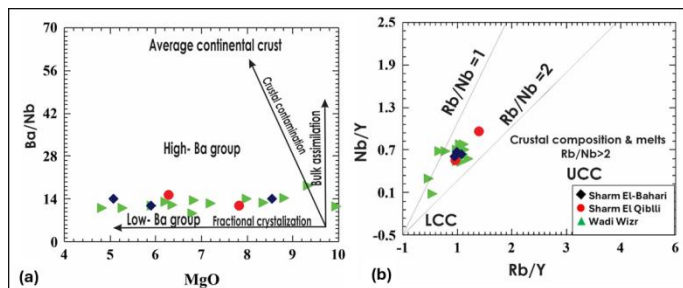


Figure 16: (a) Plotting of the analyzed samples on MgO vs. Ba/Nb variation diagrams for the studied basaltic samples. Solid line vectors show the expected trends for fractional crystallization and crustal contamination/assimilation and (b) Nb/Y vs. Rb/Y diagram for the GSR basalts (modified after [30]). Average, upper (UCC) and lower (LCC) continental crust compositions are from [24].

7.3. Magma source characteristic:

Continental intraplate basalts are frequently the product of partial melting of the upper mantle during extension of the lithosphere and consequent conventional upwelling of the asthenosphere [32] or when a mantle plume impings on the base of the continental lithosphere [33] that causes partial melting, melt segregation and finally initialing rifting. some of the authors suggest that there is a common source for the OIB and continental basalt due to similarity. such source may be represented by well-mixed convective lithosphere. To infer the characteristic source of the investigated basalts, the analyzed basalt samples are plotted on the Rb/Sr—SiO₂ diagram (Fig. 17a) [34,35]. It is observed that these samples fall within the range field of OIB, providing an additional argument for their derivation from the OIB-source mantle, which is different from the lower and upper crust.

7.4. Degree of partial melting:

The distribution of HFSE is due to the amount of garnet and pyroxene residual in the mantle Source. Different degrees

of partial melting could be displayed by the primordial mente-normalized pattern (Fig. 17b) [36], where the depletion of Y indicates garnet residual in the source. The lack of negative HFSE anomalies suggests no evidence of lithosphere Subduction signature [37]. The obtained normalized profiles are more or less similar due to the presence of Nb except for sample number and Sr peaks relative to the depletion of LILE (such as Rb, Ba, Th and U). Most samples are characterized by positive Sr anomaly, which may indicate higher degrees of partial melting. The detected negative K anomaly is attributed to the retention of K-bearing minerals such as mica and/or K-rich amphibole in the source reservoir during low degrees of partial melting. crustal contamination of most basalts is completely excluded due to the presence of negative Pb anomaly. Relationship to the East-African Rift Valley (Afro-Arabian rift system):

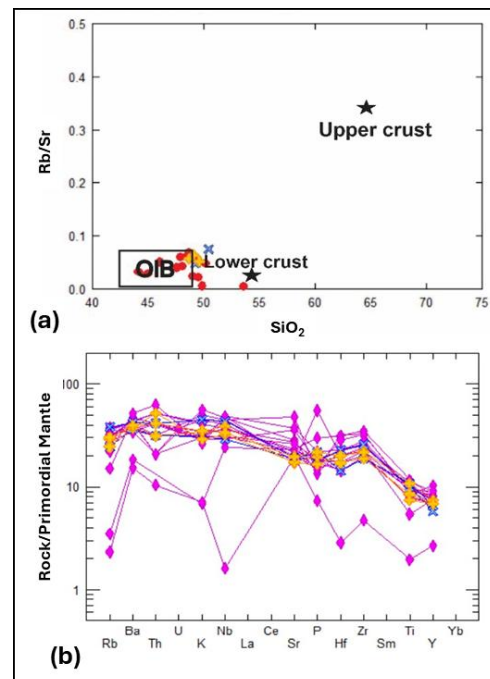


Figure 17: (a) Plotting of the analyzed samples on SiO₂ vs. Rb/Sr for the Shalatein basalts compared with OIB [34] and upper and lower crust [35] and (b) Primordial mantle-normalized patterns [36].

It is imperative to relate the investigated basalts to the Afro-Arabian rift system (Yemen, Ethiopia and Kenya) [38] mentioned that the volcanic activities in this area began in the late Eocene (44-38 Ma) and Continued until 16 Ma. He added that subsequent uplift occurred at about 5 Ma, where the second phase of volcanic activity was associated with the seafloor spreading of the Red Sea at about 4.5 Ma. In Saudi Arabia, the period of volcanic activity, known as harrats, began from 30-12 Ma. This volcanicity is attributed to a large mantle plume centered on the Afar triangle in Ethiopia (white and Mckenzie, 1989) [39]. The trace elements ratios of the studied basalts provide an argument for their derivation from the OIB-Source mantle. Thus, the model for hot asthenosphere source in the region south of Qusier city (Sharm El Bahari, Sharm El Qibli and Wizr areas) involves convective flow emanating from the Afar mantle plume in Ethiopian to produce elongated and extended lobe of hot asthenosphere beneath

northeastern Africa and Arabia [40]. Therefore, the Red Sea region is one of the youngest continental intraplate basaltic provinces where magma was generated due to lithosphere extension and mantle plume activity [6,41]. Although the studied basalts have a common Source with the OIB (i.e., they were generated from mantle plumes), radiogenic isotope studies must evaluate their source.

8. Conclusion

The following conclusions are deduced: 1. Investigated basalts form lava flow preserved within oligocene-Miocene sediments. 2. Petrographically, they are porphyritic, olivine, pyroxene, and plagioclase Phenocrysts and display vesicular and amygdaloidal types. 3. The variation in basalt composition is attributed to different degrees of partial melting and fractional crystallization. 4. The studied basalts show a limited range of SiO₂, consequently have normative quartz, and rarely contain normative nepheline. 5. Gechemically, its magma types are transitional from alkaline to tholeiitic, representing an orogenic within the plate environment. 6. There is no evidence of crustal contamination, but it is more similar to OIB.

CRediT authorship contribution statement:

Conceptualization, A.M.Asran, A.A.El-Shater and S.Rizk; methodology, Y.M.Taher; software Y.M.Taher; validation, A.M.Asran, A.A.El-Shater; formal analysis, A.M.Asran and Y.M.Taher; investigation, A.M.Asran, A.A.El-Shater; resources, A.M.Asran; data curation, S.Rizk; writing—original draft preparation, Y.M.Taher; writing—review and editing, A.M.Asran and A.A.El-Shater; visualization, A.M.Asran; supervision, A.M.Asran and A.A.El-Shater; project administration, No; funding acquisition, No. All authors have read and agreed to the published version of the manuscript.

Data availability statement

The data used to support the findings of this study are available from the corresponding author upon request.

Declaration of competing interest

The authors declare that they have no known competing financial interests or personal relationships that could have appeared to influence the work reported in this paper.

References

- [1] G.Andrew, *Bull.Fac.Sci. Egypt.Cario Univ.*,10 (1937) 1-44.
- [2] R. Said: The geology of Egypt. Elsevier publ .Co., Amsterdam and New York, (1962).
- [3] H.Schandelmeier, P.O.Reynolds: Paleogeographic Paleotectonic atlas of North-Eastern Africa. Arabia and adjacent areas. Rotterdam, Netherlands, Balkema (1997) .
- [4] M.R. Moufti, A.M. Moghazi, K.A. Ali., *Gondwana Research*, 21 (2012) 670-689.
- [5] D. Bosch, P. Verdoux ,R.C.Maury,M. El Azzouzib, C.Bollingerd, H. Bellonb, *Lithos*, 205 (2014) 247-265.
- [6] Y.Weinstein, Z. Garfunkel., *Dead Sea Transform Fault System: Reviews*, 6 (2014) 91-108.
- [7] M.F. El-Ramly, M.K. Akaad, *Geol. Surv. Egypt*, (1960) 1-33.
- [8] A.H.Sabet, Geology and mineral deposits of Gabal El-Sibai area, Red Sea Hills, Egypt. Ph.D. thesis, Leiden State University, The Netherland, (1961) 188.
- [9] M. K.Akaad, A.Noweir, *Bull. Inst. Applied Geol.*, 4 (1980) 127-135.
- [10] A.M. Noweir, M.F. Ghoneim, M.A. El-Anwar, *Proceedings of the 5th International Conference on Basement Tectonics*, (1983) 76-83.
- [11]] M.A.M. El-Anwar, *M.Sc. Thesis, Tanta Univ.*, (1983) 322.
- [12] A.A. Khudeir, A.H. Asran., *Bull. Fac. Sci. Assiut Univ.*, 21(1992) 1-22.
- [13] T. M.Mahran. *Bull.Fac.Sci.,Assiut Univ.*, 23 (1994) 551-576.
- [14] H. Kuno, *Bull. Volc.*, 20 (1959) 37-76 .
- [15] E. A. K., *Middlemost, Earth Science Reviews.*, 37(1994) 215-224.
- [16] M. A. Peacock, *Journal of Geology*, 39(1931) 54-67.
- [17] G. A. MacDonald, T. Katsura, *Journal of Petrology*, 5(1964) 83-133.
- [18] H. Kuno, *Journal of Petrology* 1 (1960)121-145.
- [19] H.Kuno, *Bull. Volcanol.*, 29 (1966) 195-222.
- [20] J.A.Winchester, P.A.Floyd, *Earth Planet.Sci. Lett.*, 28 (1976) 459-469.
- [21] T. N. Irvine, W. R. A Baragar., *Canadian Journal of Earth Sciences*, 8 (1971)523-548.
- [22] H.A.Powers, *Geochim., Cosmochim.Acta.*, 7 (1955) 77-107.
- [23] H. S. J. Yoder, C. E. Tilley, *Journal of Petrology*, 3 (1962) 342-532.
- [24] J.A. Pearce, M.J. Norry, *Contrib Mineral.Petrol.*, 69 (1979) 33-47.
- [25] M. A . Meschede, *Chemical Geology*, 56 (1986) 207-218.
- [26] J.A. Pearce, G.H., Gale, *Inst. Min. Metall. Geol Soc. Lond. Spec. Publ.*, 7 (1977) 14-24.
- [27] Pearce et al., *Earth and Planetary Science Letters*, 24 (1975) 419-426.
- [28] T.H, Green, *Tectonophysics*, 63 (1988) 367-385.
- [29] J.P. Davidson, M.A. Dungan, K.M. Ferguson, M.T. Colucci, *Geology*, 15 (1988) 443- 446.
- [30] G.Chazot, H. Bertrand, *Lithos*, 36 (1995) 69-83.
- [31] R.L.Rudnick, S. Gao, *Treatise on Geochemistry, Elsevier-Pergamon, Oxford*, 3 (2003) 1-64.
- [32] A.D. Saunders, M. Storey, R.W. Kent, M.J. Norry, *Geological Society of London Special Publication*, 68 (1992) 41-60.
- [33] J. H. CAMPBELL, R. W.GRIFFITHS, *Earth and Planetary Science Letters*, 99 (1990) 79-93.
- [34] J. G. FITTON, H. M. DUNLOP, W. P. LEEMAN, *Journal of Geophysical Research*, 96 (1991) 13,693-13711.
- [35] S. R. TAYLOR, S. M. MCLENNAN, *Oxford: Blackwell*, 122 (1985) 673-674.
- [36] P.E Holm, *Chem. Geol.*, 51(1985) 303-323.
- [37] J. A. PEARCE, *Continental basalt and mantle xenoliths*, (1983) 230-249 .
- [38] P. MOHR, *Nature*, 303 (1983) 577-584.
- [39] R. WHITE, D.MCKENZIE, *Journal of Geophysical Research*, 94 (1989) 7685-7729.
- [40] V. E. CAMP, M. J. ROOBOL, *Journal of Geophysical Research*, 97 (1992) 15255-15271.
- [41] J.Hopp, T.M. rieloff, R.Altherr, *Earth and Planetary Science Letters*, 219 (2004) 61-76.